Cooperative Optimization of Velocity Planning and Energy Management for Connected Plug-in Hybrid Electric Vehicles

Yonggang Liu[a], Zhenzhen Huang[a], Jie Li[a], Ming Ye[b], Yuanjian Zhang[c] and Zheng Chen[d, e, *]

[a]State Key Laboratory of Mechanical Transmissions & School of Automotive Engineering, Chongqing University, Chongqing 400044, China

[b]Key Laboratory of Advanced Manufacture Technology for Automobile Parts, Ministry of Education, Chongqing University of Technology, Chongqing 400054, China

[c]Sir William Wright Technology Center, Queen's University Belfast, Belfast, BT9 5BS, United Kingdom

[d]Faculty of Transportation Engineering, Kunming University of Science and Technology, Kunming 650500, China

[e]School of Engineering and Materials Science, Queen Mary University of London, London, E1 4NS, United Kingdom

Correspondence: chen@kust.edu.cn (Z. Chen) and andylyg@umich.edu (Y. Liu)

Abstract: In this paper, a cooperative optimization strategy is proposed for velocity planning and energy management of intelligent connected plug-in hybrid electric vehicles. Based on the established vehicle model, a mathematical analytical method is investigated to convert the driving cycles from the original time based profiles to the driving distance based speed values. Then, the iterative dynamic programming is exploited to achieve the synergistic optimization in terms of speed planning and power allocation of the vehicle with the consideration of gear shifting limits and speed fluctuation. To meet the requirement of trip duration limitation which may be violated due to autonomous speed planning, the terminal driving time is constrained by adding a time adjustment factor to the cost function. The simulation results suggest that the proposed strategy attains the collaborative optimization with high efficiency in terms of speed planning and driving power distribution. In addition, the proposed strategy leads to significant reduction of the energy consumption cost under the constraints of allowed speed variation ranges.

Key Words: Collaborative optimization, energy management strategy, iterative dynamic programming, plug-in hybrid electric vehicles, termination constraints.

Nomenclature

Abbreviations

A-ECMS	adaptive equivalent fuel consumption minimization strategy
BEVs	battery electric vehicles
BPNN	back propagation neural networks
CAV	connected and automated vehicle

CD	charge-depletion
CS	charge-sustaining
DCT	dual clutch transmission
DP	dynamic programing
ECMS	equivalent fuel consumption minimization strategy
EMS	energy management strategy
GPS	global positioning system
HEVs	hybrid electric vehicles
HWFET	highway fuel economy test
ICE	internal combustion engine
IDP	iterative dynamic programming
IOVs	internet of vehicles
ISG	integrated starter-generator
ITS	intelligent transportation systems
LSTM	long short time memory
MECU	mobile edge computation unit
MPC	model predict control
NEDC	new European driving cycle
NN	neural networks
P-ECMS	predictive equivalent fuel consumption minimization strategy
PHEVs	plug-in hybrid electric vehicles
PMP	Pontryagin's minimum principle
RBFNN	radial basis function neural network
RL	reinforcement learning
SOC	state of charge
SQP	sequential quadratic programming
SVM	support vector machine
UDDS	urban dynamometer driving schedule
VCUs	vehicle control units
V2I	vehicle-to-infrastructure
WT	wavelet transform

Symbols

P_{req}	required driving power of vehicle
F_f	rolling resistance
F_w	air resistance
F_i	slope resistance
F_j	acceleration resistance

m	vehicle mass
g	gravity acceleration
f	rolling resistance coefficient
α	slope of road
C_D	air resistance coefficient
A	frontal area
v	vehicle speed
δ	rotational mass coefficient
a	vehicle acceleration
P_e	engine power
P_m	motor power
T_e	engine torque
T_m	motor power
i_m	transmission ratio of torque synthesizer
i_g	transmission ratio
η_T	average efficiency of the mechanical transmission system
r_{wh}	wheel radius
b_e	fuel consumption rate
B	fuel consumption of the engine per hour
n_e	engine rotational speed
ψ	two-dimensional linear interpolation function
η_e	engine efficiency at standard atmospheric pressure
E_{low}	low calorific value of gasoline quality
P_{m_out}	output power when the motor is driving the vehicle
P_{wh}	power of the driving wheels
η_T	efficiency of the transmission system
T_{wh}	torque of the driving wheels
n_{wh}	rotational speed of the driving wheels
P_{m_in}	input power when the motor is driving the vehicle
n_m	rotational speed of the motor
$P_{m\_\max}$	max power of the motor
η_m	motor efficiency
P_b	output power of the battery
I	battery current
U	terminal voltage of the battery
E	battery electromotive force
R	internal resistance of the battery

SOC_0	initial value of state of charge
Q_b	battery capacity
N	the number of steps
r	grid midpoint
s	initial grid size
x	state variable
u	control variable
ξ	the number of grid points for state variable
χ	the number of grid points for control variable
γ	initial compressing factor
η	restoration factor
M	total iteration amount
j	current iteration
R_{in}	initial control area
R	current control area
k	current step
u_{opt}	the matrix that stores the optimal control variables
x_{opt}	the matrix that stores the optimal state variables
$d(k)$	the distance at step k
$Q_e(k)$	fuel consumption cost of each step
α_{fuel}	unit price of fuel
$Q_m(k)$	electricity cost of each step
α_{elec}	unit price of electricity
$u(k)$	decision function at step k
v_e	the speed at the end of step k
v_b	the speed at the beginning of step k
$SOC(k)$	the SOC value at step k
$x_{k\_max}^{q+1}$	upper bounds of the state variables of the iteration $q+1$
$x_{k\_min}^{q+1}$	lower bounds of the state variables of the iteration $q+1$
$x_{k\_opt}^{q}$	optimal state variables of the iteration q
$u_{k\_opt}^{q}$	optimal control variables of the iteration q
$u_{k\_max}^{q}$	upper bounds of the control variables of the iteration q
$u_{k\_min}^{q}$	lower bounds of the control variables of the iteration q

α	contraction ratios of state variables
β	contraction ratios of control variables
SOC_{max}	the SOC upper limits
SOC_{min}	the SOC lower limits
$T_{e\_max}(n_e(k))$	maximum values of engine torque at $n_e(k)$
$T_{e\_min}(n_e(k))$	minimum values of engine torque at $n_e(k)$
$T_{m\_max}(n_m(k))$	upper boundaries of the motor torque at $n_m(k)$
$T_{m\_min}(n_m(k))$	lower boundaries of the motor torque at $n_m(k)$
$T_{brake}(k)$	mechanical braking torque
$i_{\max}$	the highest gear of the transmission
$v_{\min}(k)$	lower speed limit at step k
$v_{max}(k)$	upper speed limit at step k
$a_{min}(k)$	minimum acceleration at step k
$a_{max}(k)$	maximum acceleration at step k
$vn(k)$	state transition of the speed from the beginning to the end
$Q_g(k)$	penalty cost of shifting at step k
nan	a null value
G_{no}	optimal gear at the beginning of the next step
G_c	gear at the current step
$Q_a(k)$	penalty cost of speed fluctuation at step k
A_{no}	optimal acceleration at the beginning of the next step
A_c	current acceleration
b	penalty value of speed fluctuation
J	total cost
$L(k)$	decision-making cost of each step
δ_t	time adjustment factor
D	terminal distance
t_f	final time
ΔQ	corrected fuel consumption cost
ΔSOC	difference between the ending SOC of D-EMS and that of Co-EMS
ζ	gravity of fuel
η_c	average charging efficiency of the whole trip

1. Introduction

Nowadays, electrification dominates the main development directions in vehicle industry, and battery electric vehicles (BEVs) and hybrid electric vehicles (HEVs) are two widely-accepted representatives of the existing

solutions. Due to insufficient charging facilities and so-called driving range anxieties in terms of BEVs, plug-in HEVs (PHEVs), as an extension of HEVs, remain intensively popularized because of the merged advantages of certain all-electric driving mileages (functioned as BEVs) and preferable fuel economy by means of proper energy allocation (operated as HEVs) between battery and internal combustion engine (ICE). Nonetheless, the sophisticated powertrain inside of PHEVs complicates the design of control scheme, which, also referred to as energy management strategy (EMS), accounts for power allocation between different energy sources. Distinctly, EMS plays a critical role in fuel efficiency improvement of PHEVs and has been widely investigated by industry and academia. To date, a variety of algorithms have been proposed and employed in energy management of PHEVs, and they can be grouped into three types: rule based algorithms, optimization based algorithms and data driven based algorithms.

Rule based strategies, as the name implies, can decide the operation modes and energy distribution scheme of power sources according to the characteristics of each component [1]. They can be further classified into deterministic rule strategies [2] and fuzzy rule strategies designed according to expert knowledge or engineering practice [3]. The advantages of rule based strategies are stable, robust, and easy to implement with less storage size and calculation intensity [4]. One typical rule based strategy for PHEVs is the ordinary charge-depletion/charge-sustaining (CD/CS) scheme [5]. Even various rule based strategies are spurred to improve the overall controlling performance; it is, however, still far from optimum, as the complex powertrain structures of PHEVs and incomplete knowledge of driving information lead to the difficulties of conducting proper energy allocation all the time by expert based rule strategies.

Optimization based strategies can be categorized into global optimization strategies and instantaneous optimization ones. When the future driving conditions are known, and the entailed driving power is deterministic in advance, the energy management can be treated an optimal control problem, and thus be solved by global optimization strategies. As for instantaneous optimization strategies, they often determine the optimal energy distribution with the goal of minimizing fuel consumption or energy loss instantaneously, or in a short horizon, in the premise of satisfying the driving power requirements [6]. The main difference between these two kinds of strategies is apparent. The global strategies account for the overall operation range and exploit optimal theories to achieve the global optimization, while the instantaneous ones mainly focus on the local optimization effect sustaining in a short period or transform the global optimization problem into a local optimization target. Global optimization strategies can be represented by dynamic programing (DP) [7], Pontryagin's minimum principle (PMP) [8] and quadratic programming [9]. The conventional instantaneous optimization algorithms include the equivalent fuel consumption minimization strategy (ECMS) [10], its extensions (such as adaptive ECMS (A-ECMS) and predictive ECMS (P-

ECMS)), model predictive control (MPC) [11] and reinforcement learning (RL) [12]. Ref. [13] compares different route-based EMSs for PHEVs based on different levels of trip information obtained through intelligent transportation system (ITS) and global positioning system (GPS). In it, A-ECMS and MPC are employed to split the power, respectively; followed by the optimal SOC planning based on known trip information. Ref. [14] builds up a novel hierarchical MPC based energy management framework, in which the wavelet transform (WT) and the radial basis function neural network (RBFNN) are employed cooperatively to achieve the speed prediction, and then the MPC is applied to deliver instantaneous energy allocation. Ref. [15] attempts to improve the robustness of EMSs with the combination of machine learning and the optimal EMS, and the reinforcement learning method is employed to devise a predictive EMS. Through building the transition probability function under different driving cycles, the Q-learning algorithm, as a representative of reinforcement learning algorithms, is successfully applied to attain the energy management optimization [16]. Additionally, deep reinforcement learning is also advanced to tackle the energy management of PHEVs [17].

With the development of communication technologies and data processing capabilities, connected and automated technologies have emerged to further promote fuel savings of PHEVs. Mechatronics and new informatics are integrated by these enabling technologies to provide more inputs for improving the fuel economy and operation efficiency of PHEVs [18]. In this context, the operation state of vehicles and the road information can be easily shared among drivers, manufacturers and transport segment [19].As such, data driven methods have increasingly emerged to excavate the hidden laws existing in energy management schemes. Typical solution manners include neural networks (NN), such as back propagation NN (BPNN) [20], Elman NN [21], feedforward NN [22] and long short time memory (LSTM) [23], support vector machine (SVM) [24] and regression methods [25]. In fact, the essence of data driven methods is to probe into the hidden rules of offline optimal solutions by linear/ nonlinear data fitting or regression technologies, thus transforming the offline results into online principles with a cluster of deterministic expressions or a black-box model [26]. Obviously, they are time-consuming when conducting training, and furthermore massive storage space requirement and burdensome calculation intensity are usually indispensable. Additionally, as the connected PHEVs can realize autonomous driving and speed planning with the development of internet of vehicles (IOVs) and ITS [27]. Under this circumstance, the detailed road information cannot only be accessed by PHEVs to promote energy management performance, but provide opportunities for speed planning owing to the ease of accessing surrounding driving information. This undoubtedly supplies a potential opportunity to further improve fuel economy of PHEVs. A body of researches have been spurred to investigate speed planning individually or along with energy management [28]. With the assumption of acquiring driving route ahead of

departure, Ref. [29] formulates the fuel consumption function with the horizontal input of driving distance (referred to as space domain), rather than in time domain (meaning that the horizontal input is time), and then minimizes the fuel cost by DP. Due to the complex constraints and nonlinear cost function, Ref. [30] adopts DP to cope with the speed limit caused by front vehicles and road limitations, and successfully solves out the optimal speed profile. In [31], a subsection optimization method is imported to achieve the lowest energy consumption of vehicle in a certain time and distance interval with the reduced computation amount. Ref. [32] considers the constraints in terms of gear shifting, speed limit and ramp, and exploits an improved PMP to optimize the speed profile, thereby reducing the calculation time and attaining the approximate optimal solution.

For joint optimization, usually, the controller is hierarchically divided into two layers: the vehicle layer (also called the external layer) where the speed curve is autonomously planned by the target vehicle based on the specific driving environment, and the powertrain layer (the inner layer) where the energy is allocated among power sources under the planned speed curve. The external layer is implemented to find the optimal speed curve subject to the constraints including traffic signal timing and following distance. Then, the optimized speed curve will be referred to facilitate the energy distribution in the inner layer. By assuming that the target vehicle closely follows the traffic flow, Ref. [33] proposes a speed optimization method that enables the vehicle to first accelerate and then decelerate in the controlling time domain. Ref. [34] proposes an integrated interconnected eco-driving algorithm to plan the optimal speed trajectory with smooth acceleration, which contributes to power distribution in each predicted time domain. In [35], a data-driven hierarchical EMS is proposed, which includes the optimal state of charge (SOC) planning and powertrain control of PHEVs. To generate the reference trajectory, the SOC curve is planned based on a variety of historical optimal SOC trajectories. Then, the ECMS is applied to properly allocate the energy distribution. Although the hierarchical optimization can reduce the computation cost during the control process, the coupling relationship between vehicle speed and torque distribution is not properly tackled during optimization, and thus the collaborative optimization of speed planning and torque distribution cannot be attained. The research from the Department of Energy, United States, reveals that more fuel savings can be anticipated if the vehicle-level and powertrain-level control can be optimized concurrently [36]. With the help of preview traffic information, Ref. [37] optimizes the power split ratio and speed trajectory simultaneously based on PMP. To further improve the fuel efficiency, the sequential quadratic programming (SQP) [38] and MPC are applied synthetically to plan the speed trajectory and energy allocation according to the rolling updated traffic information [39].

Typically, when all operating conditions are deterministic, DP can be exploited to achieve global optimization of energy management. However, the computation cost and memory storage requirement required by DP highly

depend on the discretization degree of state variables and control (action) variables. The cost and size will increase extremely (usually exponentially) with the dimension augment of variables. Obviously, DP is not suitable for optimizing nonlinear control problems with multiple state and control variables. To cope with this shortcoming, Ref. [40] proposes an iterative dynamic programming (IDP) algorithm which is proved efficient when solving optimization problems with high-dimensional nonlinear continuous inputs/outputs. The IDP can discretize the continuous systems based on time and space domain, and all state variables can be divided into a group of grids corresponding to the feasible values of control variables in different domain. The iteration actions are applied to compensate the system error caused by discretization, and the algorithm uses relatively sparse discrete control variables to avoid heavy computation cost during each iteration. By this manner, the optimal control sequence can be attained through a few of iterations to approximate the global optimal solution. In [41], IDP is harnessed to obtain the optimal control trajectory for a specified driving cycle. During the iterative process, an improved shifting strategy is designed to trade off fuel economy and driving performance. Ref. [42] proposes a novel cooperative EMS for PHEVs. According to the collected traffic information, the optimal battery SOC trajectory is efficiently planned by the IDP in MECUs, and subsequently the MPC is employed in on-board VCUs to resolve the final energy management by tracking the designed SOC trajectory. Ref. [43] applies the IDP method to the dynamic optimal control of HEV within an NMPC framework. The exploited IDP integrates a novel iteration manner into the conventional DP, thereby delivering an approximate optimal solution with better operation efficiency. To reduce the calculation complexity, the control problem is partitioned into a fast search for the velocity trajectory design (first order IDP) and the torque distribution (third order IDP). As can be found, the torque distribution is always attained after the velocity planning. Obviously, the method shows certain similarity with the hierarchical optimization. Furthermore, a cumbersome challenge lies in that the space domain solution proposed in [43] cannot satisfy the requirement of the constrained terminal driving time.

In summary, there exists seldom research, to the authors' knowledge, on how to coordinately optimize autonomous speed planning and energy management to further promote energy savings of connected PHEVs. This, therefore, becomes the main research focus in this study. Actually, the cooperative optimization is a dual variable optimization problem with an accumulated target (fuel economy maximization) and subject to a series of restrictions, such as speed and driving duration limitation. The current mainstream output is supplied based on the space domain, followed by time domain and time-space based solutions. In this study, the collaborative optimization is continually conducted in space domain, including autonomous speed planning and energy distribution under speed limit conditions. To attain it, a mathematical method is proposed to convert the speed limit based driving contour in time

domain into that in space domain. Then, the IDP is employed to achieve the collaborative optimization for connected PHEVs. However, the space domain solution usually cannot satisfy the constrained terminal driving time. To cope with it, an adjustment factor is introduced to ensure reaching the destination with the preset driving duration. Finally, the simulation results highlight the feasibility of the proposed collaborative optimization scheme in terms of speed planning and energy management. The main contributions of this study can be attributed to the following three aspects: 1) a mathematical analytical method is proposed to directly convert the time-domain speed limit condition into the non-uniform discrete speed demand in space domain; 2) the IDP is efficiently applied in speed planning and energy management of connected PHEVs; 3) an effective adjustment algorithm is introduced to ensure that the trip during resulted from speed planning meet the preset threshold.

The remainder of this paper is organized as follows: In Section II, the powertrain structure and system model are detailed. In Section III, the collaborative optimization strategy is built based on IDP in space domain, and the method of terminal state constraint is investigated. The simulation validations are carried out in Section IV. Finally, the main conclusions are drawn in Section V.

2. Powertrain structure and system model

In this paper, a parallel PHEV is targeted as the research object, of which the powertrain topology is shown in Fig. 1, where an engine and an integrated starter-generator (ISG) are coaxially connected. There exists a dual clutch transmission (DCT) between the motor and the main reducer. By controlling the engagement/ disengagement of the main clutch as well as the status of engine and motor, six operating modes can be defined, including pure electric driving, engine driving, hybrid driving, driving charging, parking charging and regenerative braking [44]. To design the co-optimization strategy, the vehicle longitudinal dynamics and the main powertrain component modeling need to be addressed.

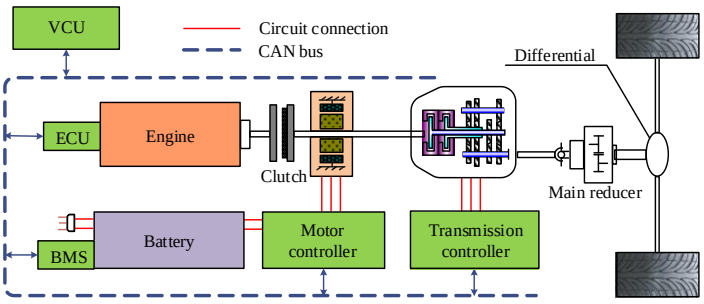

Fig. 1. Powertrain system of parallel plug-in hybrid electric vehicle.

2.1. *Vehicle Longitudinal Dynamic Model*

The tractive force ordered by the driver is transmitted to wheels to overcome the driving resistance. The required driving power of vehicle P_{req} can be formulated as:

$$P_{req} = (F_f + F_w + F_i + F_j) \cdot \frac{v}{3600} \tag{1}$$

$$P_{req} = (P_e + P_m) \cdot \eta_T \tag{2}$$

where the rolling resistance $F_f = m \cdot g \cdot f \cdot \cos\alpha$, the air resistance $F_w = \frac{C_D \cdot A \cdot v^2}{21.15}$, the slope resistance $F_i = m \cdot g \cdot \sin\alpha$, the acceleration resistance $F_j = \delta \cdot m \cdot a$, m expresses the vehicle mass, g is the gravity acceleration and equals 9.8 m/s^2, f represents the rolling resistance coefficient, α indicates the slope of road, C_D expresses the air resistance coefficient, A denotes the frontal area, v is the vehicle speed, δ expresses the rotational mass coefficient, a denotes the vehicle acceleration, P_e indicates the engine power, P_m represents the motor power. The tractive force transmitted to wheels can be calculated as:

$$F_t = \frac{(T_e + T_m \cdot i_m) i_g \cdot \eta_T}{r_{wh}} \tag{3}$$

where T_e denotes the engine torque, T_m indicates the motor power, i_m denotes the transmission ratio of torque synthesizer, i_g expresses the transmission ratio, η_T is the average efficiency of the mechanical transmission system, and r_{wh} represents the wheel radius.

2.2. *Engine model*

In this study, a fuel consumption model is used to characterize the fuel consumption rate of the engine. It is obtained by interpolating the experimental data with the steady-state operation data. The current fuel consumption rate can be obtained by interpolation of engine torque and rotational speed, as shown in Fig. 2. The engine fuel consumption rate can be calculated by:

$$b_e = \frac{B}{P_e} \cdot 1000 \tag{4}$$

where b_e expresses the fuel consumption rate (unit: g/(kW·h)), and B denotes the fuel consumption per hour (unit: kg/h). The engine power P_e can be formulated, as:

$$P_e = \frac{T_e \cdot n_e}{9550} \tag{5}$$

where n_e represents the engine rotational speed. From (4) and (5), the fuel consumption rate can be calculated, as:

$$b_e = 9550000\frac{B}{T_e \cdot n_e} = \psi(T_e \cdot n_e) \tag{6}$$

where ψ denotes a two-dimensional linear interpolation function in terms of engine torque and rotational speed, as shown in Fig. 2.

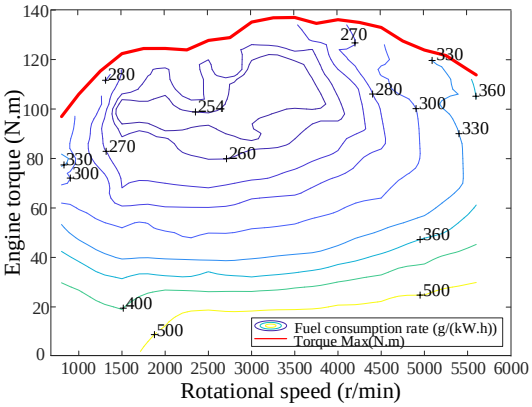

Fig. 2. Engine consumption model.

2.3. *ISG model*

The ISG can convert either electric energy exported from the battery to mechanical energy to drive the vehicle, or the mechanical energy generated during braking to electric energy. The motor model mainly includes the external rotational speed/torque characteristics and the operation efficiency, both of which are calibrated in the testbed. The maximum power curve can be acquired based on the torque and rotational speed variation, as shown in Fig. 3 (a). The motor efficiency model can be expressed as a function of motor torque and rotational speed fitted by the spline interpolation, as shown in Fig. 3 (b). The motor power can be calculated, as:

$$P_{m\_out} = \frac{P_{wh}}{\eta_T} = \frac{T_{wh} \cdot n_{wh}}{9550\eta_T} \tag{9}$$

$$P_{m\_in} = \frac{T_m \cdot n_m}{9550} \tag{10}$$

$$P_{m\_\max} = \max(P_{m\_out}, P_{m\_in}) \tag{11}$$

where P_{m_out} expresses the outputted power propelling the vehicle, P_{wh} denotes the demanded power on the wheel, η_T is the transmission efficiency, T_{wh} represents the wheel torque, n_{wh} denotes the rotational speed of wheels, P_{m_in} expresses the inputted power when the motor drives the vehicle, n_m denotes the rotational speed of the motor, and $P_{m\_\max}$ expresses the maximum power of the motor. Consequently, combining (9) and (10), the motor efficiency η_m can be calculated, as:

$$\eta_m = \frac{P_{out}}{P_{in}} \cdot 100\% = \psi(T_m \cdot n_m) \tag{12}$$

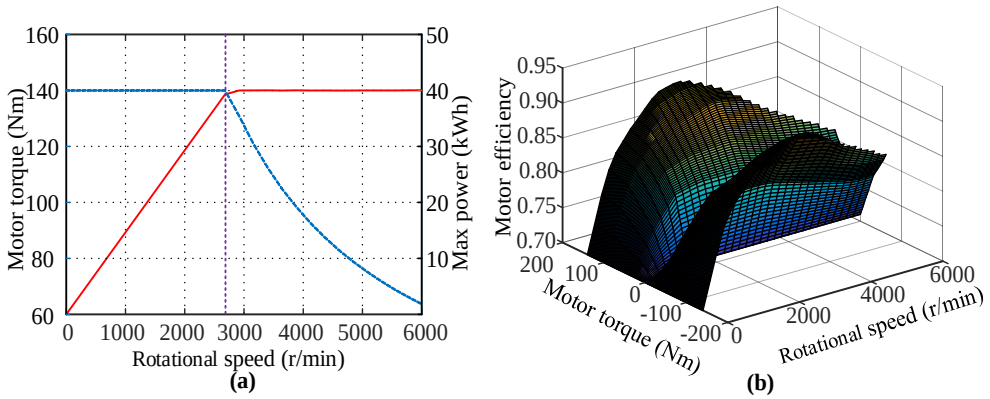

Fig. 3. ISG model. (a) ISG external characteristic curve; (b) ISG efficiency.

2.4. *Battery model*

In this study, a simple but effective resistance model is adopted to describe the battery's electric performance, as widely employed in literature [45]. The battery's electromotive force and internal resistance are mainly affected by SOC and temperature. However, only the influence from SOC is considered in this paper for simplicity, and the temperature and aging influence is neglected. By means of interpolation fitting, the test data from the hybrid pulse power characterization experiment is utilized to generate an empirical model that can describe the relationship about the internal resistance and electromotive force with regard to SOC, as shown in Fig. 4.

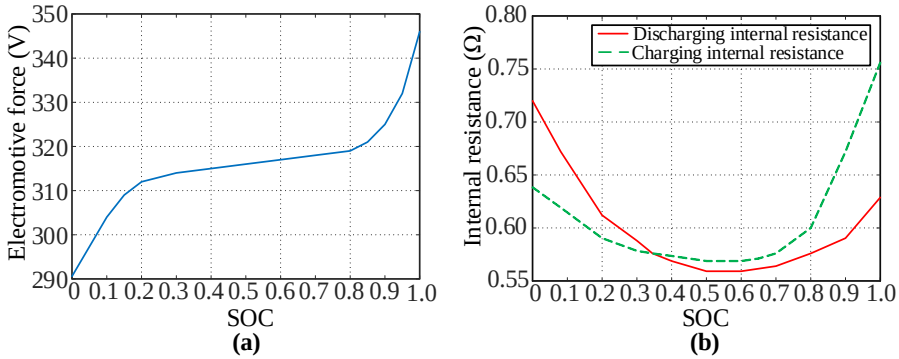

Fig. 4. The electromotive force and internal resistance of battery. (a) Electromotive force; (b) Internal resistance.

When the battery is discharged, the batter output power P_b is:

$$P_b = I \cdot U \tag{13}$$

where I is the battery current, and U denotes the terminal voltage of the battery. According to the Kirchhoff's law, the terminal voltage of the battery U can be calculated by:

$$U = E - I \cdot R \tag{14}$$

where E denotes the battery electromotive force, and R represents the internal resistance. According to (13) and (14), I can be calculated, as:

$$I = \frac{E - \sqrt{E^2 - 4RP_b}}{2R} \tag{15}$$

The battery SOC is an important parameter that reflects the battery's remaining capacity and can influence the energy management performance to a large extent. In this paper, the ampere-hour integration method is employed to calculate the SOC [46], as:

$$SOC(t) = SOC_0 - \frac{\int_0^t I(t)dt}{Q_b} \tag{16}$$

where SOC_0 represents the initial value of SOC, and Q_b indicates the battery capacity.

Based on the detailed modeling preparation, the proposed cooperative optimization framework will be elaborated to achieve both the speed planning and energy management.

3. Design of collaborative optimization algorithm

When designing the EMS, two assumptions are made in this study, including that 1) the speed limit information of vehicle can be acquired online due to the network connected property of the studied PHEV, and 2) the speed can be independently planned during driving. By determining the decision function, state transfer function, constraint condition and the objective function, the co-optimization of speed planning and torque distribution is tackled to optimize the fuel economy under speed restrictions. The framework of the proposed EMS is sketched in Fig. 5. As can be found, the IDP is exploited based on the given speed limitations and the constructed PHEV model to supply the optimized velocity and torque distribution.

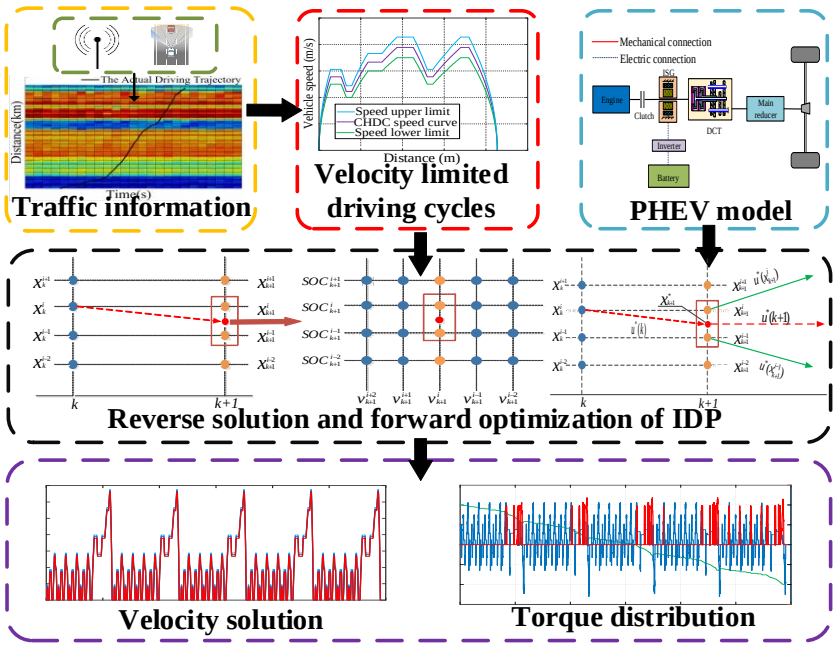

Fig. 5. Framework of the proposed collaborative optimization EMS.

3.1. *Iterative dynamic programming*

Given the deterministic global speed curves, DP, as an effective global optimization algorithm, has been widely leveraged in energy management of PHEVs. However, due to the intensive computation labor and large storage requirement, it is intractable to directly apply DP to conduct the co-optimization work. To accelerate the optimization and lessen the exponentially increased storage size, the IDP is introduced by reducing the searching grid of optimal trajectory to attain the same, or approximate, optimization effect, as shown in Fig. 6. The application of IDP algorithm includes the following steps [43]:

Step l: Averagely partition the problem into N stages;

Step 2: Choose the grid midpoint r, the initial grid size s, the number of grid points ξ and χ for the state variable x and control variable u, and determine the initial compressing factor γ, the initial control area R_{in} and the restoration factor η;

Step 3: Determine the total iteration amount M, and set the ordinal number of current iteration $j=1$;

Step 4: Set the current control area $R=\eta^{q-1}R_{in}$;

Step 5: Calculate the state values $x(k)$ of other stages according to the initial stage's state;

Step 6: Solve the optimal control command of each period from the first stage and set the current stage $k=N-1$. Select p evenly in the control area for each control variable to comprise the current control strategy. Use the initial state $x(k)$ of current stage and the optimal control strategy of subsequent stages to calculate the states of the subsequent stages and acquire the performance indexes. Select the control strategy corresponding to the smallest cost function as the optimal control strategy $u(k)$ at the current stage by comparing different performance indexes. Set $k=k-1$, and complete the iteration when $k=0$. Store the control strategy of the current iteration in u_{opt} and the corresponding state trajectory in x_{opt};

Step 7: Reduce the control area of the control variables $R=\gamma R$, and increase the ordinal number of iterations: $j=j+1$. When $j<M$, go to step 2 and adjust the grid range of the state variable and control variable. When $j=M$, terminate the iteration.

It can be seen from the above steps that the calculation procedure of IDP is basically the same as that of conventional DP. It starts by calculating the optimal cost function at the last stage, then step by step solves the accumulated cost function backward. The solution of each stage is determined based on the minimum result of the cost function.

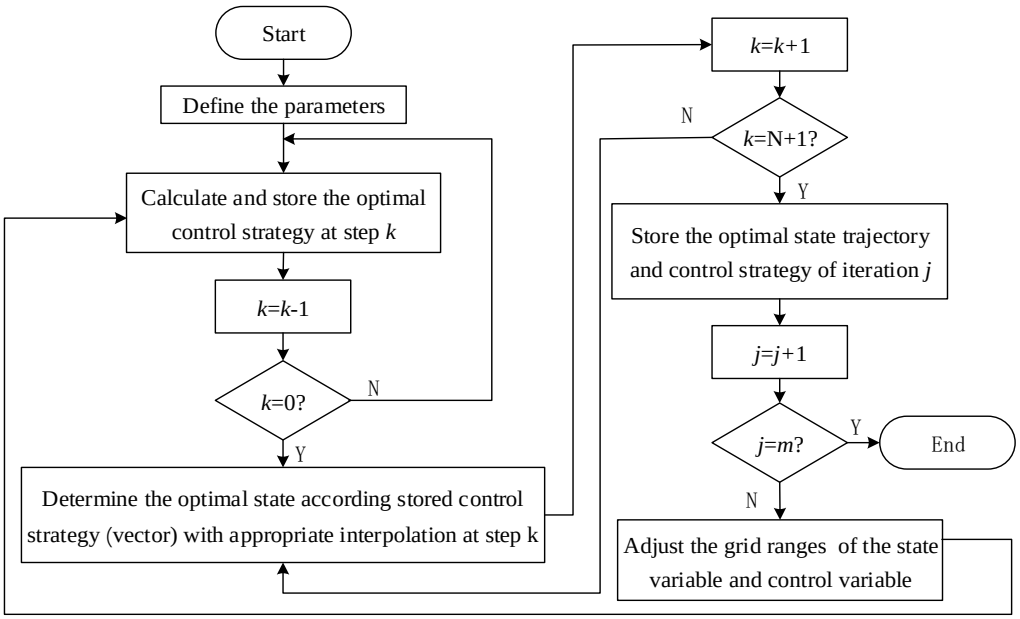

Fig. 6. The calculation process of IDP.

3.2. *Analysis of co-optimization problem*

In view of the co-optimization of speed planning and torque distribution, as most of researches are focused on tackling the fuel consumption minimization in a specific trip, it is more instinctive to consider and solve the problem in space domain. However, the supplied speed information is usually with the horizontal axis of time. For ease of conducting the optimization, firstly, the driving cycle needs to be transferred from time domain to spatial domain [47]. Taking the new European driving cycle (NEDC) as an example, it is in time domain and only provides the speed value at the end of each second and the acceleration in each second. If the speed at the end of each second is regarded as a constant during the interval, then the step change of the speed will be incurred. Furthermore, Ref. [48] shows that the length of each stage of uniform dispersion generates certain influence on accuracy of the obtained space domain operating conditions. On this account, this study proposes a mathematical method that directly converts the time domain conditions to the non-uniform discrete space domain operating conditions. The distance of each stage in the space domain driving cycle is consistent with the distance of each stage in the corresponding time domain. By doing so, it can generate proper discrete operating conditions, and the distance of each stage can be obtained by:

$$d(k+1) = d(k) + \frac{v(k) + v(k+1)}{2} \tag{17}$$

where $d(k)$ and $d(k+1)$ are the distance at step k and $k+1$, $v(k)$ and $v(k+1)$ are the speed at step k and $k+1$, respectively. Note that the direct space domain discretization cannot deal with the situation when the speed is zero. To tackle it, during the conversion process, the speed commands equaling zero in time domain driving cycle need to be removed first. Then, the points with zero speed in the corresponding position needs to be refilled

after the solution is solved. The schematic diagram of the NEDC in space domain is shown in Fig. 7. As can be found, there exist obvious difference between the speed contours.

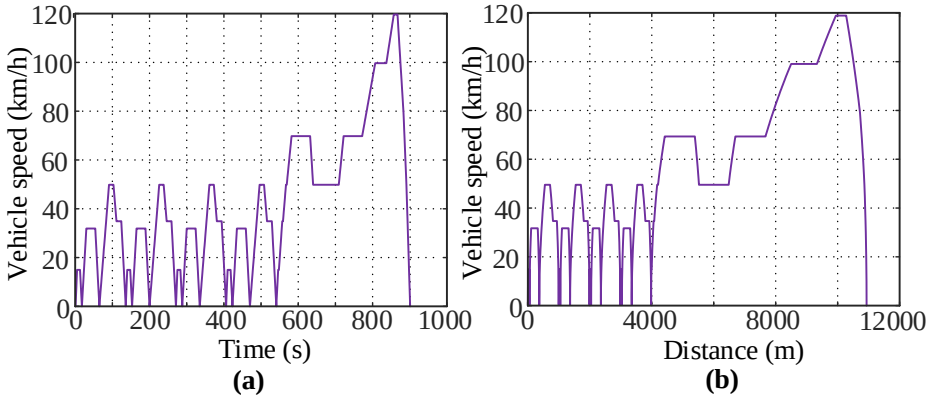

Fig. 7. The NEDC cycle under the time and space domain. (a) The time domain after removing the point where the velocity is zero; (b) The space domain which is non-uniformly discrete.

As mentioned before, this paper aims to simultaneously optimize the vehicle speed and energy distribution ratio, where the energy distribution can be regarded as the torque distribution, as after determining the engine torque, the whole torque distribution can be assigned correspondingly. Actually, the vehicle speed is correlated with the vehicle acceleration. As such, the acceleration and engine torque are chosen as the control variables. In addition, the fuel consumption cost and electric energy consumption cost are related to the rotational speed, as:

$$Q_e(k) = \frac{\alpha_{fuel} \cdot B(k)}{3600} = \frac{\alpha_{fuel} \cdot b_e \cdot T_e \cdot n_e}{3600 \cdot 1000 \cdot 9550} \tag{15}$$

$$Q_m(k) = \frac{\alpha_{elec} \cdot T_m \cdot n_m}{3600} \tag{16}$$

where $Q_e(k)$ represents the fuel consumption cost at step k, α_{fuel} is the unit price of fuel, $B(k)$ denotes the fuel consumption of the engine per hour, $Q_m(k)$ expresses the electricity cost, and α_{elec} is the unit price of electricity. Among them, the rotational speed can be influenced by the gear ratio, as:

$$n_e = n_m = \frac{v \cdot i_g}{0.377 \cdot r_{wh}} \tag{17}$$

where i_g denotes the transmission ratio, which should also be controlled during the solving process. Thus, the engine torque T_e, the transmission ratio i_g and acceleration a are selected as the control variables. In addition, the speed and SOC are both selected as the state variables, and the state transition function can be expressed as:

$$\begin{cases} SOC(k+1) = SOC(k) - \dfrac{I(k)}{Q_b} \\ v(k+1) = \sqrt{2 \cdot a(k) \cdot d(k) + v^2(k)} \end{cases} \tag{18}$$

where $SOC(k)$ and $SOC(k+1)$ indicate the SOC value at step k and $k+1$. $I(k)$ expresses the battery current at step k, Q_b indicates the battery capacity, $v(k)$ and $v(k+1)$ indicate the speed value at step k and $k+1$, $a(k)$ denotes the current acceleration at step k. In the first iteration, the optimal trajectory is calculated in the low-precision control grids and state grids. The generated trajectory will be used as the grid's center for subsequent iterations. It should be noted that the grid size gradually increases in each iteration. Thus, the interval between grid points is reduced, and the grid becomes smoother in each iteration. The related functions for adjusting the grid size of state variables and control variables can be expressed as:

$$\begin{cases} x_{k\_\min}^{q+1} = \max(x_{k\_\min}^{q}, x_{k\_opt}^{q} - \alpha(x_{k\_\max}^{q} - x_{k\_\min}^{q})) \\ x_{k\_\max}^{q+1} = \min(x_{k\_\max}^{q}, x_{k\_opt}^{q} + \alpha(x_{k\_\max}^{q} - x_{k\_\min}^{q})) \\ u_{k\_\min}^{q+1} = \max(u_{k\_\min}^{q}, u_{k\_opt}^{q} - \beta(u_{k\_\max}^{q} - u_{k\_\min}^{q})) \\ u_{k\_\min}^{q+1} = \min(u_{k\_\max}^{q}, u_{k\_opt}^{q} + \beta(u_{k\_\max}^{q} - u_{k\_\min}^{q})) \end{cases} \tag{19}$$

where $x_{k\_max}^{q+1}$ and $x_{k\_min}^{q+1}$ represents the upper and lower bounds of the state variables in step k of iteration $q+1$, $u_{k\_max}^{q}$ and $u_{k\_opt}^{q}$ denote the optimal state variables and the optimal control variables in step k of iteration q, $u_{k\_max}^{q}$ and $u_{k\_min}^{q}$ express the upper and lower bounds of the control variables in step k of iteration q, α and β are contraction ratios of state variables and control variables. In addition, the following constraints should be satisfied, as:

$$\begin{cases} SOC_{min} \le SOC(k) \le SOC_{max} \\ n_{e\_min} \le n_e(k) \le n_{e\_max} \\ T_{e\_min}(n_e(k)) \le T_e(k) \le T_{e\_max}(n_e(k)) \\ n_{m\_min} \le n_m(k) \le n_{m\_max} \\ T_{m\_min}(n_m(k)) \le T_m(k) \le T_{m\_max}(n_m(k)) \\ T_{req}(k) = T_e(k) + T_m(k) + T_{brake}(k) \\ i_g(k), i_g(k+1) \in \{1,2,3,4,5,6\} \\ n \in \{1,3,5\} \\ i_g(k+1) = \begin{cases} i_g(k)+1, & \text{when upshifting,} \\ i_g(k+1) = i_g(k) - n, & \text{when downshifting.} \end{cases} \\ v_{\min}(k) \le v(k) \le v_{\max}(k) \\ a_{\min}(k) \le a(k) \le a_{\max}(k) \\ v_{\min}(k+1) \le vn(k) \le v_{\max}(k+1) \end{cases} \tag{20}$$

where SOC_{max} and SOC_{min} are the SOC upper and lower limits which are set to prevent overcharge and over discharge of the battery, $n_e(k)$ denotes the engine's rotational speed at step k, $T_{e\_max}(n_e(k))$ and $T_{e\_min}(n_e(k))$

express the maximum and minimum values of engine torque at $n_e(k)$, $n_m(k)$ indicates the motor's rotational speed at step k, $T_{m\_max}(n_m(k))$ and $T_{m\_min}(n_m(k))$ represent the upper and lower boundaries of the motor torque at $n_m(k)$, $T_{brake}(k)$ expresses the mechanical braking torque, $i_{\max}$ denotes the highest gear of the transmission, $v_{\min}(k)$ and $v_{max}(k)$ are the lower speed limit and upper speed limit at step k, $a_{\min}(k)$ and $a_{\max}(k)$ represent the minimum acceleration and the maximum acceleration at step k, $vn(k)$ denotes the state transition of the speed from the beginning to the end of step k, $v_{min}(k+1)$ and $v_{max}(k+1)$ indicate the lower speed limit and the upper speed limit at step $k+1$. Moreover, in the process of decision-making of the control variables, the frequent shifting limit of transmission and frequent fluctuation limit of vehicle speed should also be considered, as:

$$Q_g(k)=\begin{cases} nan, & \text{if } G_{no}-G_c \geq 2 \text{ or } G_{no}-G_c=\text{-}2 \text{ or } G_{no}-G_c=\text{-}4, \\ 0.0000119, & \text{if } G_{no}\neq G_c, \\ 0, & \text{otherwise.} \end{cases} \tag{21}$$

where $Q_g(k)$ denotes the penalty cost of the gear shifting at step k, nan indicates a null value, G_{no} represents the optimal gear at the beginning of the next step, G_c expresses the gear position at the current step, and 0.000119 denotes the shifting penalty value determined by trial-and-error. The speed frequent fluctuation limit is detailed as:

$$Q_a(k)=\begin{cases} \mathrm{b}\cdot\left|A_c - A_{no}\right|, & \text{if } \left|A_c\right| \geq 0.001, \\ 0, & \text{if } \left|A_c\right| < 0.001. \end{cases} \tag{22}$$

where $Q_a(k)$ expresses the penalty cost of speed fluctuation at step k, A_{no} indicates the optimal acceleration at the beginning of next step, A_c represents the current acceleration, and b denotes the penalty value of speed fluctuation. For the collaborative optimization of PHEV, the limiting condition is speed constraints. Actually, the optimization goal is to attain the optimal comprehensive energy consumption economy at all steps in the premise of meeting the speed constraints. The expression of its objective function can be formulated, as:

$$\begin{cases} J=\sum_{k=1}^{N} L(x(k),u(k)) \\ L(k)=(Q_e(k)+Q_m(k)+Q_g(k)+Q_a(k))\cdot t(k) \end{cases} \tag{23}$$

where J expresses the total cost, and $L(k)$ denotes the decision-making cost of each step.

3.3. *Terminal state constraint*

The collaborative algorithm can achieve the optimal comprehensive energy consumption economy with the speed and acceleration limits, however the cost optimization is not the only purpose of the solution. To exhibit practical significance, it should meet all the terminal state constraints which includes driving time and driving

distance. By considering the problem with constraints in three dimensions (time, distance and velocity), Ref. [49] initially proposes a three-dimensional method with high computational cost to solve this constraint problem. To reduce the calculation time, the problem is resolved by a two-dimensional method [50]. By searching all possible vehicle speed solutions at each step, finding the optimal speed trajectory and adding the time adjustment factor δ_t to the cost function, all the limits of time, distance and speed can all be satisfied. For the space domain solution, its terminal time needs to be constrained. Therefore, the cost function can be reformulated, as:

$$L(k) = (Q_e(k) + Q_m(k) + Q_g(k) + Q_a(k) + \delta_t) \cdot t(k) \tag{24}$$

Each δ_t is with an associated terminal time, and when the terminal time is fixed, δ_t is uniquely determined. According to the first order optimality conditions, the adjoint state of δ_t can be defined, as:

$$\dot{\delta}_t = \frac{\partial L(k)}{\partial t} = 0 \tag{25}$$

where δ_t is a constant. The terminal time constraint of the vehicle can be satisfied by calculating δ_t, as:

$$t(D) = t_f \tag{26}$$

where D denotes the terminal distance, and t_f indicates the final time. The method of adjusting δ_t is similar to the method of solving the zero point of function based on the dichotomy algorithm [51].

After preparing the state and control variables, the cost function and the termination conditions, the IDP is employed to conduct the simulation to validate its feasibility.

4. Simulation validation

In this study, the simulation is conducted in MATLAB/Simulink to verify the feasibility of the proposed co-optimization strategy. Since the main advantage of the proposed strategy is the collaborative optimization of speed and torque distribution, it is necessary to conduct the systematic and comprehensive validations under three working modes of PHEVs. 1) All-electric mode: in this mode, the vehicle completes the trip mainly by the electric energy, and the engine only works when the motor power cannot meet the torque demand. 2) Charge sustaining mode: the battery is near the lower threshold of SOC at the beginning of trip, and the SOC is allowed to fluctuate in a small range. 3) Blended mode: the battery starts with a high initial SOC, and the driving distance is long. However, the electric energy in the battery cannot meet the whole trip demand, and the engine is required to participate in propelling the vehicle in this mode.

The all-electric mode and charge-sustaining mode are similar to the working scheme of BEVs and HEVs. A special driving cycle (called CHDC in this study) introduced in [37] is selected as a reference, and it is converted into the driving cycle in space domain according to the method detailed in Section III. As the purpose of this paper is to achieve simultaneous speed planning and torque distribution under specific speed limit conditions, the speed upper and lower limit determination is only to simulate the actual conditions when driving on real roads, and the boundary width is not the focus of this paper. The setting method of the speed limits is similar to that in [52]. The upper limit of speed is 1.1 times larger than the standard value, and the lower limit is 90% of the standard value. Fig. 8 (a) shows the simulation speed profiles. Under the blended mode, a longer driving cycle needs to be selected to better examine the performance of the proposed strategy, and in this case, 5 consecutive NEDC cycles are continually simulated. The upper limit is set to 0.5 m/s above the normal value, and the lower limit is set to 0.5 m/s below the normal value, as shown in Fig. 8 (b). Note that although the discussed two driving cycles are selected as the basic working conditions, the adaptability of the proposed collaborative strategy in other driving cycles will be further addressed in the following study.

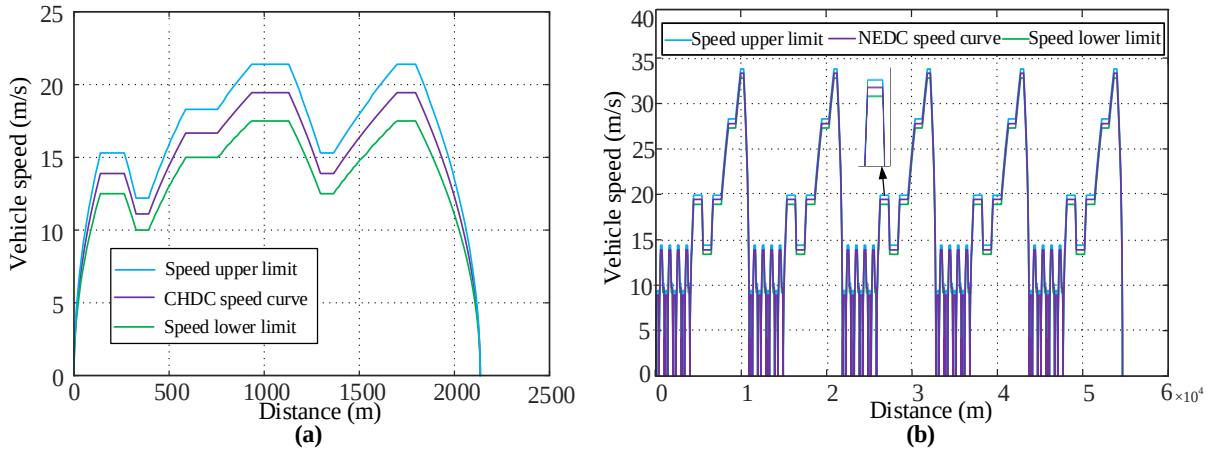

Fig. 8. Driving cycles. (a) All-electric mode and charge sustaining mode driving cycles; (b) Blended mode driving cycle.

As introduced in Section III, the stages are discretized according to the driving distance, and the distance of each stage is consistent with that in the corresponding time domain. The number of iterations is set to 15, the constant number of grid points is set to 7 for SOC, and the step-size of discretization for velocity is set to 0.2 m/s. For the NEDC cycle, the energy consumption cost over iteration for different contraction factors is shown in Fig. 9. It can be found that the objective function decreases with iteration, the global minimum can be obtained after 10 iterations most of the time. Besides, the contraction rate of 0.3 can achieve the optimal performance for the current driving cycle. Moreover, the impact of the contraction rates on the computational time of the IDP is analyzed, as shown in Fig. 10. As can be found, the computation duration increases exponentially with the increase of the contraction rate. Even so, the maximum computation is less than 400 s, which is accepted for practical applications. Note that as the

IDP is only employed in this study to attain the collaborative optimization and the algorithm itself is not our research focus, the impact of other parameters on the calculation time is not addressed with much detail.

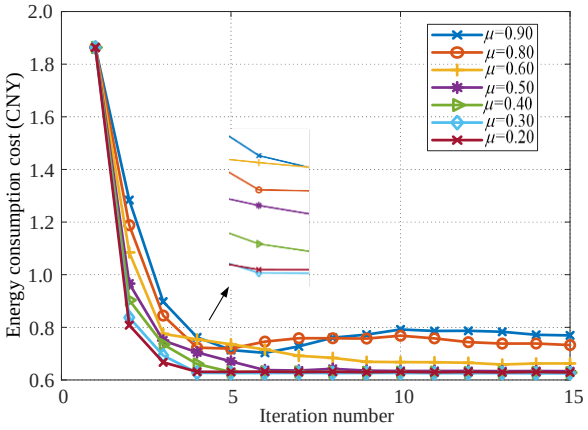

Fig. 9. Energy consumption cost over iteration number for different contraction rates.

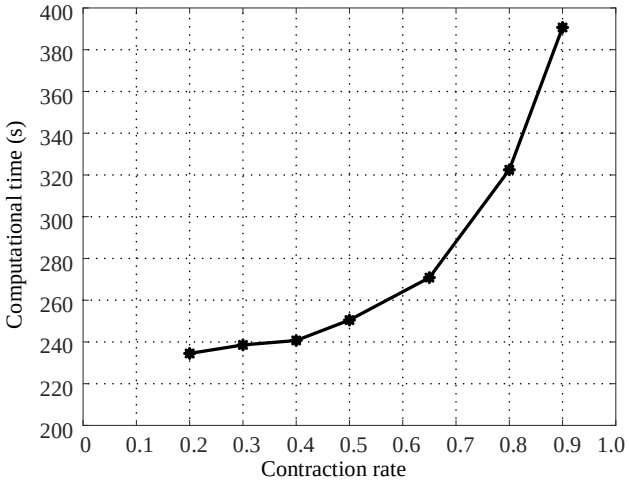

Fig. 10. Computational time for different contraction rates.

4.1. Validation under the all-electric mode

The simulation results of the collaborative optimization strategy under the all-electric mode is shown in Fig. 11. The initial SOC is set to 0.7, and the contract rate is set to 0.38. As can be seen from Fig. 11 (a), the speed planned by the collaborative optimization strategy will accelerate before the CHDC speed increases, and it will continue to decelerate after the CHDC speed deceleration stops. This proposed planning method can ensure that the driving motor works in the high-efficiency area without extra load during acceleration, and more braking energy can be recovered during deceleration. The solution speed curve is smoother than the CHDC speed curve, and distinctly the solution speed shows a close tendency to the desired speed curve. Moreover, the torque distribution of vehicle is shown in Fig. 11 (b). All the energy consumed under the all-electric mode comes from the battery. In conclusion, each control command can positively contribute to cooperative control.

To further evaluate the performance of the proposed strategy, the energy consumption cost is investigated with the following three EMS: 1) D-EMS, which is the deterministic EMS based on DP in the selected driving cycle [7],

2) Co-EMS (Unconstrained), which is the proposed cooperative optimization strategy based on IDP without the terminal state constraint, and 3) Co-EMS (Constrained), which is the proposed cooperative optimization strategy based on IDP with the terminal state constraint. Note that as the D-EMS is widely adopted in energy management of PHEVs, here the detailed introduction about D-EMS is not elaborated in this paper but can be found in [7] and the references therein. Taking the initial SOC of 0.7 as an example, the specific energy consumption cost based on the three strategies is compared in Table 1. As can be seen, compared with the D-EMS, the Co-EMS (Unconstrained) can save 14.77% energy consumption while promoting the time loss of 7.92%, and the Co-EMS (Constrained) can save 12.75% energy consumption with the time augment of 0.25%. Despite the consideration of terminal state constraint leading to slight increase of the energy consumption cost, the cooperative optimization strategy highlights superior comprehensive energy consumption economy, and it can reach the destination within the allowed time, proving its feasibility.

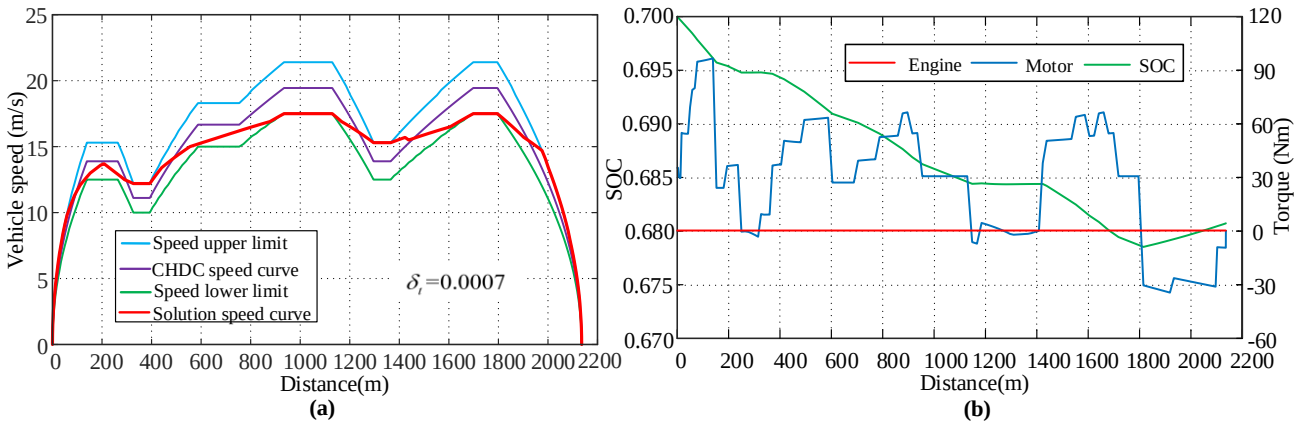

Fig. 11. Simulation results under the all-electric mode. (a) Solution speed; (b) Torque distribution.

Table 1 Comparison of energy consumption cost under the all-electric mode with the initial SOC of 0.7.

Control strategy	Electric Cost (CNY)	Total Cost (CNY)	Distance (m)	Time (s)
D-EMS	0.149	0.149	2136	159.0
Co-EMS (Unconstrained)	0.127	0.127 (↓ 14.77%)	2136	171.6 (↑ 7.92%)
Co-EMS (constrained)	0.130	0.130 (↓ 12.75%)	2136	159.4 (↑ 0.25%)

4.2. Validation under the charge sustaining mode

Fig. 12 shows the simulation results of the collaborative optimization strategy under the charge sustaining mode. The initial value and expected final value of SOC are both set to 0.3, and the contraction rate is set to 0.42. As can be seen from Fig. 12 (a), compared with the speed under the all-electric mode, the speed under the charge sustaining mode shows larger fluctuation, and the planned speed shows similar variation trend during acceleration and the sliding segment. In summary, the planned vehicle speed includes a relatively large acceleration, which is beneficial for keeping the engine load stable and improving its working efficiency. In addition, smooth deceleration can attain

the reasonable maintenance of electric energy. As can be seen from Fig. 12 (b), the torque of engine and motor is relatively stable, and these two power sources can work harmoniously. Moreover, the SOC varies gently throughout the trip and reaches the expected final value at the end of trip. In general, the proposed strategy under the charge sustaining mode can better realize the cooperative control, and the torque distribution between two energy sources is more proper. As the ending SOC of D-EMS and Co-EMS cannot be exactly the same when their costs are compared under the charge sustaining mode, the fuel consumption of D-EMS is corrected by the equivalent fuel cost, as:

$$\Delta Q = \Delta SOC \cdot Q_b \cdot b_e \cdot \alpha_{fuel} \cdot g / (\zeta \cdot \eta_c) \tag{31}$$

where ΔQ denotes the corrected fuel consumption cost, ΔSOC indicates the difference between the ending SOC of D-EMS and that of Co-EMS, ζ denotes the gravity of fuel and equals the product of density and gravity acceleration, η_c expresses the average charging efficiency of the whole trip, which is acquired by calculating the ratio of the motor and battery power at all charging points. Table 2 lists the energy consumption cost based on the three strategies. As can be seen, compared with the D-EMS, the Co-EMS (Unconstrained) saves 13.22% energy consumption but improves the driving duration by 4.84%, and the Co-EMS (Constrained)) saves the energy consumption by 12.42% and the time cost by 0.82%. Even the energy consumption cost saved by the cooperative optimization strategy under the charge sustaining mode is slightly less than that under the all-electric mode, the preferable energy consumption and time cost still manifest the feasibility of the proposed co-optimization algorithm.

Table 2 Comparison of energy consumption cost under the charge sustaining mode with the initial SOC of 0.3.

Control strategy	Ending SOC	Corrected Cost (CNY)	Distance (m)	Time (s)
D-EMS	0.2992	0.628	2136	159.0
Co-EMS(Unconstrained)	0.2993	0.545 (↓ 13.22%)	2136	166.7 (↑ 4.84%)
Co-EMS(Constrained)	0.2990	0.550 (↓ 12.42%)	2136	160.3 (↑ 0.82%)

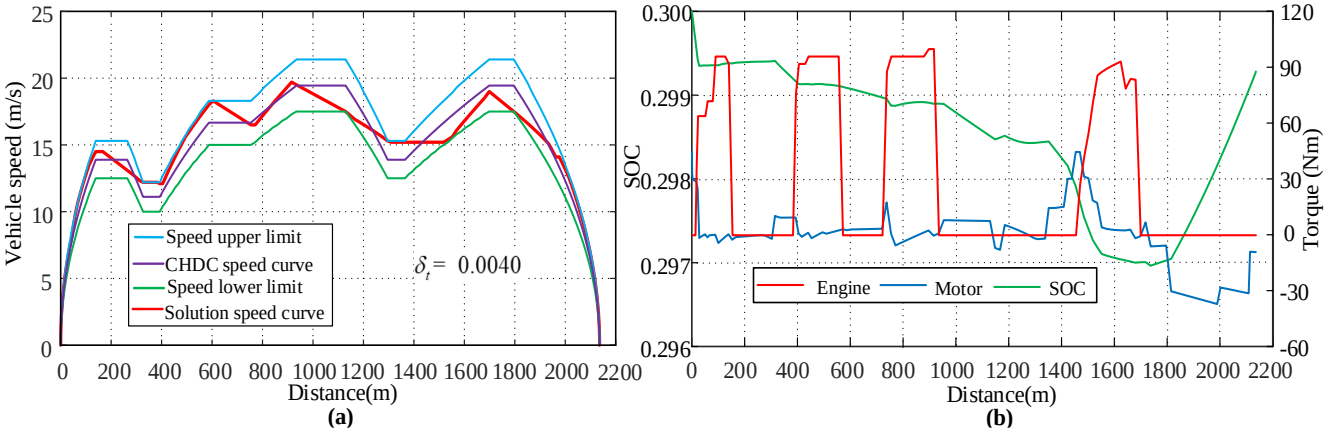

Fig. 12. Simulation results under the charge sustaining mode. (a) Solution speed; (b) Torque distribution.

4.3. Validation under the blended mode

Fig. 13 shows the simulation results under the blended mode when the initial SOC is set to 0.7. As can be seen

from Fig. 13 (a), the solving speed tends to be higher than the NEDC profile when the overall speed limit is less than 10 m/s. However, when the speed limit values are higher than 10 m/s, the speed curve gradually follows the speed lower limit. The achieved speed curve helps to ensure that the engine can work under a relatively moderate load. Fig. 13 (b) shows the torque distribution of the vehicle and the SOC trajectory. As can be found, the SOC changes uniformly throughout the trip and falls near the lower limit value of SOC at the end of the trip. The proposed strategy under the blended mode can realize the cooperative control of input variables. The speed curve is smoother than the NEDC speed profile. Table 3 compares the energy consumption cost based on three strategies. Compared with the D-EMS, the Co-EMS (Unconstrained) saves 7.32% energy consumption with the time reduction of 3.82%, and the Co-EMS (Constrained) saves 6.81% energy consumption with the time reduction of 0.62%. Note that the optimization effect of the energy consumption cost also depends on the specified speed limit range. A larger speed limit range can certainly achieve better energy consumption economy. From this point of view, both Co-EMSs can finish the co-optimization job with superior performance, and the Co-EMS (Unconstrained) performs slightly better than the Co-EMS (Constrained) in terms of no matter energy consumption or time cost.

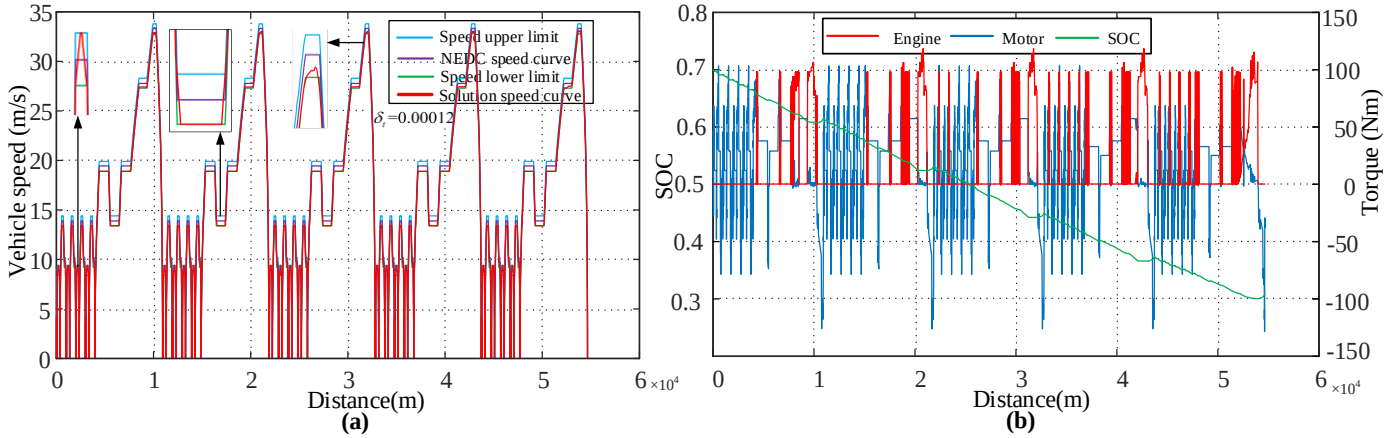

Fig. 13. Simulation results under the blended mode. (a) Solution speed; (b) Torque distribution.

Table 3 Comparison of energy consumption cost under the blended mode with the initial SOC of 0.7.

Control strategy	Electric Cost (CNY)	Fuel Cost (CNY)	Total Cost (CNY)	Distance (km)	Time (s)
D-EMS	2.57	7.12	9.69	54.66	5925.00
Co-EMS (Unconstrained)	2.57	6.04	8.98 (↓ 7.32%)	54.66	6151.49 (↑ 3.82%)
Co-EMS (Constrained)	2.57	6.46	9.03 (↓ 6.81%)	54.66	5962.23 (↑ 0.62%)

In addition, the influence of different driving cycles on the optimization effect of the proposed strategy is also examined. To ensure that the driving distance exceeds the all electric driving distance, 8 consecutive urban dynamometer driving schedule (UDDS) driving cycles and 6 consecutive highway fuel economy test (HWFET) driving cycles are selected in this study. The energy consumption cost based on the three strategies under the two

driving cycles are shown in Table 4, and the initial SOC is also set to 0.7. In the UDDS cycle, compared with the D-EMS, the proposed Co-EMS (Unconstrained) saves 10.85% energy consumption with the time reduction of 4.13%, and the Co-EMS (Constrained)) saves 9.22% energy consumption with the time increment of 0.45%. While in the HWFET cycle, compared with the D-EMS, the Co-EMS (Unconstrained) can save 9.86% energy consumption with the time loss of 5.29%. These results manifest that the proposed collaborative optimization strategy enables the vehicle to reach the destination within the specified time and with higher fuel economy under different driving cycles.

Table 4 Comparison of energy consumption cost in UDDS and HWFET with the initial SOC of 0.7.

Driving Cycle	Control strategy	Electric Cost (CNY)	Fuel Cost (CNY)	Total Cost (CNY)	Distance (km)	Time (s)
UDDS	D-EMS	2.61	2.92	5.53	59.60	10960.00
	Co-EMS (Unconstrained)	2.61	2.32	4.93 (↓10.85%)	59.60	11412.53 (↑4.13%)
	Co-EMS (Constrained)	2.61	2.41	5.02 (↓9.22%)	59.60	11009.86 (↑0.45%)
HWFET	D-EMS	2.61	3.78	6.39	61.54	4596.00
	Co-EMS (Unconstrained)	2.61	3.15	5.76 (↓9.86%)	61.54	4839.12 (↑5.29%)
	Co-EMS (Constrained)	2.61	3.26	5.87 (↓8.14%)	61.54	4612.80 (↑0.36%)

To sum up, the proposed collaborative optimization strategy can achieve autonomous planning of speed curve, and cooperative torque distribution in the premise of constraining the terminal state under the three working modes. Compared with the D-EMS, the comprehensive energy consumption economy of the proposed collaborative strategy is significantly improved. Moreover, the energy consumption economy of the collaborative optimization strategy is also justified under different driving cycles.

5. Conclusions

This paper proposes a collaborative optimization energy management strategy based on iterative dynamic programming for intelligent connected plug-in hybrid electric vehicles. The collaborative optimization strategy based on iterative dynamic programming is designed in space domain to achieve the simultaneous speed planning and torque distribution. By adding the time adjustment factor to the cost function, the vehicle can reach the destination with the expected driving time, thus advancing the practical significance of the control strategy. The simulation results show that the proposed cooperative optimization energy management strategy can realize the cooperative control of each input variable effectively. Compared with the traditional energy management strategy, the proposed collaborative optimization energy management strategy can respectively reduce the energy consumption cost by 12.75%, 12.42%, and 6.81% under all-electric, charge sustaining and blended modes, thus verifying the advantages and effectiveness of the proposed strategy. Additionally, the proposed collaborative optimization energy management

strategy is not only applicable to connected plug-in hybrid electric vehicles, but also applicable to other intelligent connected vehicles.

However, it is worth noting that the computational cost of the proposed energy management strategy is still high. Hence, the following research will concentrate on improving the calculation efficiency when applying in practice. Moreover, in terms of energy management of intelligent connected plug-in hybrid electric vehicles, this paper only makes a systematic study on iterative dynamic programming based on the specific driving cycles. The feasibility of the proposed strategy under the real driving environment will also be investigated in the future.

Acknowledgements

This work was supported in part by the National Natural Science Foundation of China (No. 51775063 and No. 61763021), in part by the National Key R&D Program of China (2018YFB0105402), and in part by the EU-funded Marie Skłodowska-Curie Individual Fellowships Project under Grant 845102-HOEMEV-H2020-MSCA-IF-2018.

References

[1] A. Neffati, S. Caux, M. Fadel, Fuzzy switching of fuzzy rules for energy management in HEV, IFAC Proceedings Volumes. 45 (2012) 663-668, https://doi.org/10.3182/20120902-4-FR-2032.00116.
[2] S.F. Tie, C.W. Tan, A review of energy sources and energy management system in electric vehicles, Renewable and Sustainable Energy Reviews. 20 (2013) 82-102, https://doi.org/10.1016/j.rser.2012.11.077.
[3] S. Ahmadi, S.M.T. Bathaee, A.H. Hosseinpour, Improving fuel economy and performance of a fuel-cell hybrid electric vehicle (fuel-cell, battery, and ultra-capacitor) using optimized energy management strategy, Energy Conversion And Management. 160 (2018) 74-84, https://doi.org/10.1016/j.enconman.2018.01.020.
[4] Y. Liu, J. Li, Z. Chen, D. Qin, Y. Zhang, Research on a multi-objective hierarchical prediction energy management strategy for range extended fuel cell vehicles, Journal of Power Sources. 429 (2019) 55-66, https://doi.org/10.1016/j.jpowsour.2019.04.118.
[5] Y. Wang, X. Wang, Y. Sun, S. You, Model predictive control strategy for energy optimization of series-parallel hybrid electric vehicle, Journal of Cleaner Production. 199 (2018) 348-358, https://doi.org/10.1016/j.jclepro.2018.07.191.
[6] B. Geng, J.K. Mills, D. Sun, Energy Management Control of Microturbine-Powered Plug-In Hybrid Electric Vehicles Using the Telemetry Equivalent Consumption Minimization Strategy, Ieee Transactions on Vehicular Technology. 60 (2011) 4238-4248, https://doi.org/10.1109/Tvt.2011.2172646.
[7] S. Xie, F. Sun, H. He, J. Peng, Plug-In Hybrid Electric Bus Energy Management Based on Dynamic Programming, Energy Procedia. 104 (2016) 378-383, https://doi.org/10.1016/j.egypro.2016.12.064.
[8] L. Tribioli, R. Cozzolino, D. Chiappini, P. Iora, Energy management of a plug-in fuel cell/battery hybrid vehicle with on-board fuel processing, Applied Energy. 184 (2016) 140-154, https://doi.org/10.1016/j.apenergy.2016.10.015.
[9] Z. Chen, C.C. Mi, R. Xiong, J. Xu, C. You, Energy management of a power-split plug-in hybrid electric vehicle based on genetic algorithm and quadratic programming, Journal of Power Sources. 248 (2014) 416-426, https://doi.org/10.1016/j.jpowsour.2013.09.085.
[10] A. Rezaei, J.B. Burl, B. Zhou, Estimation of the ECMS Equivalent Factor Bounds for Hybrid Electric Vehicles, Ieee Transactions on Control Systems Technology. 26 (2018) 2198-2205, https://doi.org/10.1109/Tcst.2017.2740836.
[11] C. Xiang, F. Ding, W. Wang, W. He, Energy management of a dual-mode power-split hybrid electric vehicle based on velocity prediction and nonlinear model predictive control, Applied Energy. 189 (2017) 640-653, https://doi.org/https://doi.org/10.1016/j.apenergy.2016.12.056.
[12] B. Xu, F. Malmir, D. Rathod, Z. Filipi, Real-Time Reinforcement Learning Optimized Energy Management for a 48V Mild Hybrid Electric Vehicle, SAE Technical Paper Series, 2019.
[13] A. Taghavipour, M. Vajedi, N.L. Azad, J. McPhee, A Comparative Analysis of Route-Based Energy Management Systems for Phevs, Asian J Control. 18 (2016) 29-39, https://doi.org/10.1002/asjc.1191.
[14] Z. Chen, N. Guo, J. Shen, R. Xiao, P. Dong, A Hierarchical Energy Management Strategy for Power-Split Plug-in Hybrid Electric Vehicles Considering Velocity Prediction, IEEE Access. 6 (2018) 33261-33274, https://doi.org/10.1109/access.2018.2848464.
[15] X. Hu, T. Liu, X. Qi, M. Barth, Reinforcement Learning for Hybrid and Plug-In Hybrid Electric Vehicle Energy Management: Recent Advances and Prospects, IEEE Industrial Electronics Magazine. 13 (2019) 16-25, https://doi.org/10.1109/mie.2019.2913015.
[16] G. Du, Y. Zou, X. Zhang, Z. Kong, J. Wu, D. He, Intelligent energy management for hybrid electric tracked vehicles using online reinforcement learning, Applied Energy. 251 (2019), https://doi.org/10.1016/j.apenergy.2019.113388.

[17] Y.W.A. C, H.T.B. C, J.P.A. C, H.Z.B. C, H.H.A. D, Deep reinforcement learning of energy management with continuous control strategy and traffic information for a series-parallel plug-in hybrid electric bus, Applied Energy. 247 (2019) 454-466, https://doi.org/10.1016/j.apenergy.2019.04.021.
[18] F.Q. Zhang, X.S. Hu, R. Langari, D.P. Cao, Energy management strategies of connected HEVs and PHEVs: Recent progress and outlook, PrECS. 73 (2019) 235-256, https://doi.org/10.1016/j.pecs.2019.04.002.
[19] R. Xiong, Y.Z. Zhang, H.W. He, X. Zhou, M.G. Pecht, A Double-Scale, Particle-Filtering, Energy State Prediction Algorithm for Lithium-Ion Batteries, Ieee Transactions on Industrial Electronics. 65 (2018) 1526-1538, https://doi.org/10.1109/Tie.2017.2733475.
[20] S. Xie, X. Hu, S. Qi, K. Lang, An artificial neural network-enhanced energy management strategy for plug-in hybrid electric vehicles, Energy. 163 (2018) 837-848, https://doi.org/10.1016/j.energy.2018.08.139.
[21] R. Liu, D. Shi, C. Ma, Real-Time Control Strategy of Elman Neural Network for the Parallel Hybrid Electric Vehicle, Journal of Applied Mathematics. 2014 (2014) 1-11, https://doi.org/10.1155/2014/596326.
[22] J. Moon, S. Park, S. Rho, E. Hwang, A comparative analysis of artificial neural network architectures for building energy consumption forecasting, International Journal of Distributed Sensor Networks. 15 (2019), https://doi.org/10.1177/1550147719877616.
[23] K. Yeon, K. Min, J. Shin, M. Sunwoo, M. Han, Ego-Vehicle Speed Prediction Using a Long Short-Term Memory Based Recurrent Neural Network, International Journal of Automotive Technology. (2019),
[24] A. Jindal, N. Kumar, M. Singh, Internet of energy-based demand response management scheme for smart homes and PHEVs using SVM, Future Generation Computer Systems. (2018), https://doi.org/10.1016/j.future.2018.04.003.
[25] Y. Zhang, L. Chu, Y. Ding, N. Xu, C. Guo, Z. Fu, L. Xu, X. Tang, Y. Liu, A Hierarchical Energy Management Strategy Based on Model Predictive Control for Plug-In Hybrid Electric Vehicles, Ieee Access. 7 (2019) 81612-81629, https://doi.org/10.1109/access.2019.2924165.
[26] C. De Cauwer, W. Verbeke, T. Coosemans, S. Faid, J. Van Mierlo, A Data-Driven Method for Energy Consumption Prediction and Energy-Efficient Routing of Electric Vehicles in Real-World Conditions, Energies. 10 (2017), https://doi.org/10.3390/en10050608.
[27] A. Sciarretta, G. De Nunzio, L.L. Ojeda, Optimal Ecodriving Control Energy-Efficient Driving of Road Vehicles as an Optimal Control Problem, Ieee Contr Syst Mag. 35 (2015) 71-90, https://doi.org/10.1109/Mcs.2015.2449688.
[28] H. Liu, X. Li, W. Wang, L. Han, C. Xiang, Markov velocity predictor and radial basis function neural network-based real-time energy management strategy for plug-in hybrid electric vehicles, Energy. 152 (2018) 427-444, https://doi.org/10.1016/j.energy.2018.03.148.
[29] J. Wollaeger, S.A. Kumar, S. Onori, D. Filev, U. Ozguner, G. Rizzoni, S. Di Cairano, Cloud-computing based Velocity Profile Generation for Minimum Fuel Consumption: A Dynamic Programming based Solution, P Amer Contr Conf. (2012) 2108-2113,
[30] F. Mensing, E. Bideaux, R. Trigui, H. Tattegrain, Trajectory optimization for eco-driving taking into account traffic constraints, Transport Res D-Tr E. 18 (2013) 55-61, https://doi.org/10.1016/j.trd.2012.10.003.
[31] W. Dib, A. Chasse, P. Moulin, A. Sciarretta, G. Corde, Optimal energy management for an electric vehicle in eco-driving applications, Control Engineering Practice. 29 (2014) 299-307, https://doi.org/10.1016/j.conengprac.2014.01.005.
[32] E. Ozatay, U. Ozguner, D. Filev, Velocity profile optimization of on road vehicles: Pontryagin's Maximum Principle based approach, Control Engineering Practice. 61 (2017) 244-254, https://doi.org/10.1016/j.conengprac.2016.09.006.
[33] T.S. Kim, C. Manzie, H. Watson, Fuel Economy Benefits of Look-ahead Capability in a Mild Hybrid Configuration, IFAC Proceedings Volumes. 41 (2008) 5646-5651, https://doi.org/https://doi.org/10.3182/20080706-5-KR-1001.00952.
[34] X. Qi, G. Wu, P. Hao, K. Boriboonsomsin, M.J. Barth, Integrated-Connected Eco-Driving System for PHEVs With Co-Optimization of Vehicle Dynamics and Powertrain Operations, IEEE Transactions on Intelligent Vehicles. 2 (2017) 2-13, https://doi.org/10.1109/tiv.2017.2708599.
[35] H. Tian, S.E. Li, X. Wang, Y. Huang, G. Tian, Data-driven hierarchical control for online energy management of plug-in hybrid electric city bus, Energy. 142 (2018) 55-67, https://doi.org/10.1016/j.energy.2017.09.061.
[36] A. Atkinson, A. Salvia, G. Vishwanathan, Powertrain innovations for connected and autonomous vehicles. In: Proc. Powertrain Innov. Workshop, Adv. Res. Projects Agency-Energy, Denver, USA . 2015
[37] C. Zheng, G. Xu, K. Xu, Z. Pan, Q. Liang, An energy management approach of hybrid vehicles using traffic preview information for energy saving, Energy Conversion and Management. 105 (2015) 462-470, https://doi.org/10.1016/j.enconman.2015.07.061.
[38] G. Heppeler, M. Sonntag, U. Wohlhaupter, O. Sawodny, Predictive planning of optimal velocity and state of charge trajectories for hybrid electric vehicles, Control Engineering Practice. 61 (2017) 229-243, https://doi.org/10.1016/j.conengprac.2016.07.003.
[39] T.S. Kim, C. Manzie, R. Sharma, Model Predictive Control of Velocity and Torque Split in a Parallel Hybrid Vehicle, Ieee Sys Man Cybern. (2009) 2014-2019, https://doi.org/Doi 10.1109/Icsmc.2009.5346115.
[40] R. Luus, Iterative dynamic programming, Chapman and Hall/CRC2000.
[41] X. Tian, R. He, Y. Xu, Design of an Energy Management Strategy for a Parallel Hybrid Electric Bus Based on an IDP-ANFIS Scheme, Ieee Access. 6 (2018) 23806-23819, https://doi.org/10.1109/access.2018.2829701.
[42] Y. Zhang, C. Guo, G. Li, Y. Liu, Z. Chen, Cooperative control strategy for plug-in hybrid electric vehicles based on a hierarchical framework with fast calculation, Journal of Cleaner Production. 251 (2020), https://doi.org/10.1016/j.jclepro.2019.119627.
[43] H.G. Wahl, F. Gauterin, An Iterative Dynamic Programming Approach for the Global Optimal Control of Hybrid Electric Vehicles under Real-time Constraints, Ieee Int Veh Sym. (2013) 592-597,
[44] Y.G. Liu, J. Li, M. Ye, D.T. Qin, Y. Zhang, Z.Z. Lei, Optimal Energy Management Strategy for a Plug-in Hybrid Electric Vehicle Based on Road Grade Information, Energies. 10 (2017), https://doi.org/ARTN 41210.3390/en10040412.
[45] Z. Lei, D. Qin, L. Hou, J. Peng, Y. Liu, Z. Chen, An adaptive equivalent consumption minimization strategy for plug-in hybrid electric vehicles based on traffic information, Energy. 190 (2020) 116409, https://doi.org/https://doi.org/10.1016/j.energy.2019.116409.
[46] S. Bauer, A. Suchaneck, F. Puente León, Thermal and energy battery management optimization in electric vehicles using Pontryagin's maximum principle, Journal of Power Sources. 246 (2014) 808-818, https://doi.org/https://doi.org/10.1016/j.jpowsour.2013.08.020.
[47] A. Dubray, P. Beguery, Energy Management Strategy of Hybrid Electric Vehicles and Driving Cycles, IFAC Proceedings Volumes. 33 (2000) 1131-1136, https://doi.org/https://doi.org/10.1016/S1474-6670(17)39564-2.
[48] A. Lajunen, Energy-optimal velocity profiles for electric city buses, 2013 IEEE International Conference on Automation Science and Engineering (CASE), 2013, pp. 886-891.
[49] F. Mensing, R. Trigui, E. Bideaux, Vehicle trajectory optimization for application in ECO-driving, 2011 IEEE Vehicle Power and Propulsion Conference, 2011, pp. 1-6.
[50] D. Maamria, K. Gillet, G. Colin, Y. Chamaillard, C. Nouillant, Which methodology is more appropriate to solve eco-driving optimal control problem for conventional vehicles?, 2016 IEEE Conference on Control Applications (CCA), IEEE, 2016, pp. 1262-1267.
[51] R.P. Brent, An algorithm with guaranteed convergence for finding a zero of a function, Computer Journal. (1971) 4,
[52] C. Zheng, G. Xu, S.W. Cha, Q. Liang, A predictive driving control strategy of electric vehicles for energy saving, International Journal of Precision Engineering and Manufacturing. 16 (2015) 197-202, https://doi.org/10.1007/s12541-015-0026-0.